

## Giant Magnetoelastic Coupling in a Love Acoustic Waveguide Based on TbCo<sub>2</sub>/FeCo Nanostructured Film on ST-Cut Quartz

Aurélien Mazzamurro,<sup>1,\*</sup> Yannick Dusch<sup>1</sup>, Philippe Pernod,<sup>1</sup> Olivier Bou Matar,<sup>1</sup> Ahmed Addad,<sup>2</sup> Abdelkrim Talbi<sup>1</sup> and Nicolas Tiercelin<sup>1</sup>

<sup>1</sup>Univ. Lille, CNRS, Centrale Lille, Univ. Polytechnique Hauts-de-France, UMR 8520 – IEMN, F-59000 Lille, France

<sup>2</sup>Univ. Lille, CNRS, INRA, ENSCL, UMR 8207 – UMET – Unité Matériaux et Transformations, F-59000 Lille, France

(Received 2 August 2019; revised manuscript received 15 November 2019; accepted 24 January 2020; published 1 April 2020)

In this work, we propose a theoretical and experimental investigation of the interaction of *guided* pure shear-horizontal (SH) wave within a uniaxial multilayered TbCo<sub>2</sub>/FeCo thin film deposited on ST-X90°-cut quartz in a delay-line configuration. We evaluate theoretically the evolution of phase velocity as a function of magnetic field and experimentally the variation of  $S_{21}$  transmission coefficient (amplitude and phase). An equivalent piezomagnetic model based on pure magnetoelastic coupling is used (developed to allow us) to calculate the elastic stiffness constants of the multilayer as a function of the bias magnetic field. The model is also implemented for the calculation of acoustic waves' dispersion curves. We show that the evolution of the phase velocity with respect to the bias magnetic field is dominated by the  $C_{66}$  elastic stiffness constant as expected for the case of shear-horizontal surface acoustic wave. In the fabricated device, both fundamental and third-harmonic shear mode are excited at 410 MHz and 1.2 GHz, respectively. For both modes, the theoretical and experimental results are in agreement. At 1.2 GHz, the guiding of the acoustic wave in the ferromagnetic thin film enhances the sensitivity to the bias magnetic field with a maximum phase-velocity shift close to 2.5% and an attenuation reaching 500 dB/cm, for a sensitivity as high as 250 ppm/Oe, which is better than what has been reported in the literature so far. We also report that, from a specific ratio between the thin-film thickness and the acoustic wavelength, the bias magnetic field can induce a breaking of the acoustic wave polarization, leading to an acoustic mode conversion.

DOI: [10.1103/PhysRevApplied.13.044001](https://doi.org/10.1103/PhysRevApplied.13.044001)

### I. INTRODUCTION

Magnetic field sensing is widely used for numerous applications ranging from navigation and positioning systems such as inertial units, magnetic anomaly detection, to electrical current sensors or biomagnetic signals sensors such as magnetocardiography, magnetoencephalography or hepatic iron concentration. In such applications, common demands concerning the sensors' capabilities are the following: room-temperature operation, compact size for high spatial resolution or limited available space, and low power consumption. For the past few years, various approaches have emerged to fill the aforementioned criteria. Thin-film or plate-based magnetoelectric resonators [1–5] show encouraging results but their limited frequency range due to downscaling constraints reduces their potential. In the meantime, surface-acoustic-wave- (SAW) based devices have emerged as a promising technology in magnetic field sensing with the use of

magnetostrictive materials being able to convert magnetic energy to mechanical energy and vice versa. When biased with a magnetic field, strain and stress is induced in the magnetostrictive thin film due to the natural alignment of the magnetization along the external perturbation leading to elastic strain. The modification of the elastic properties of magnetostrictive composites with respect to a bias magnetic field is known as  $\Delta E/G$  effect [6–8], which reflects bulk or shear modulus variation, respectively. Typically, SAW devices are operated in a delay-line configuration [9–15] or in a resonator structure with one or two ports [16–19]. SAW devices are preferred for rf applications since downscaling and thus, frequency increase is much easier compared to magnetoelectric based resonators. In the former case, coupling between dynamic strain and magnetization was investigated by various research teams through either resonant or nonresonant interaction. In the latter, the magnetoelastic coupling induces the shift of the acoustic wave dispersion curves, whereas in resonant coupling, dynamic strain is used to induce the magnetization precession corresponding to the crossing between magnon

\*aurelien.mazzamurro@centralelille.fr

and phonon dispersion curves. In previous studies reported in the literature, nonresonant coupling was investigated with various ferromagnetic materials such as Fe-Ga, Ni, TbFe<sub>2</sub>, TbCo<sub>2</sub>, Fe-Co, or Fe-Co-Si-B using leaky or surface acoustic waves [11,15,20,21] showing sagittal (including Rayleigh waves) or transverse polarization with a penetration depth reaching few to several wavelengths, reducing accordingly the sensitivity. In particular, Li *et al.* [11] reported the design of a magnetic field sensor based on 500-nm-thick Fe-Ga film deposited on ST-cut quartz showing a maximum velocity shift of 0.64% at 158 MHz. Zhou [15] conducted the experimental and theoretical study of a SAW delay line based on multilayered TbCo<sub>2</sub>/FeCo nanostructured thin film deposited on Y-cut LiNbO<sub>3</sub>. A very good agreement is reached between theoretical predictions and experimental data, both for Rayleigh and shear mode with a maximum acoustic wave velocity shift close to 0.2%. Elhosni *et al.* [20] investigated experimentally and theoretically the use of Ni and Co-Fe-B as sensing materials in a delay-line configuration on LiNbO<sub>3</sub> YX-128° coated with ZnO. A maximum sensitivity of 16 ppm/mT is reached with Co-Fe-B at 460 MHz. Kittmann *et al.* [10] presented a Fe-Co-Si-B thin-film-coated Love-type SAW device for magnetic field sensing with a very low magnetic noise level of 100 pT/√Hz. SAW resonator structures are also investigated and noticeable results are obtained: Smole *et al.* [17] proposed a one-port resonator in a Fe-Co-Si-B/ZnO structure with a tuning range of about 1.2% at 1.2 GHz. Kadota *et al.* [19] showed the first excitation of a pure shear-horizontal surface acoustic wave on ST-X90°-cut quartz to design resonators as magnetic field sensors. A one-port resonator composed of Ni interdigital transducers (IDTs) with a sensitivity to magnetic field close to 8 ppm/Oe is designed. More recently, Liu *et al.* [18] reported classic Love acoustic waveguide in a one-port resonator with a SiO<sub>2</sub> layer and Fe-Co-Si-B as a magnetostrictive layer with a relative frequency shift of 0.5% at 220 MHz.

The coupling between dynamic strain and magnetization is also interpreted as ferromagnetic resonance (FMR) by some research teams [21–25]. Thevenard *et al.* [24] showed the dynamic strain effect on a magnetic semiconductor coated with a ZnO layer and obtained a velocity shift close to 0.007% and an attenuation close to 1 dB/cm at 549 MHz. Dreher *et al.* [21] investigated acoustic-wave-driven FMR (ADFMR) in a Ni thin film using a SAW delay-line configuration on LiNbO<sub>3</sub> at high frequency. At 170 MHz, an attenuation close to 1 dB/cm is obtained, reaching 160 dB/cm at 2.24 GHz. Labanowski *et al.* also investigated ADFMR in a Ni thin film in a delay-line configuration on Y-cut LiNbO<sub>3</sub> and an attenuation of 500 dB/cm at 2.5 GHz for a 20-nm-thick thin film was claimed by the authors. In these works, although a resonant coupling between magnetization and dynamic strain is claimed, the relative acoustic wave velocity shifts

observed with respect to the bias magnetic field remain weak compared to nonresonant coupling.

In summary, most of the studies concerning the coupling between dynamic strain and magnetization focus on leaky-type or surface acoustic wave to induce magnetization precession or pure magnetoelastic effect. The study of the true nature of this coupling presents a major challenge owing to the complex acoustic wave polarization generally used and the magnetization state of the ferromagnetic thin film. The studies concerning resonant coupling show a great interest in magnon-phonon interaction at a fundamental level, but the sensitivity with respect to the magnetic field remains weak compared to pure magnetoelastic-coupling-based devices for magnetic field-sensor applications. However, the latter devices have also a limited sensitivity due to the evanescent nature of the employed acoustic waves, a non-negligible part being radiated into the substrate. With Love wave devices, the confinement of the acoustic wave is better but only a small part travels in the ferromagnetic layer coated on the silicon dioxide. In order to enhance the sensitivity, improving the confinement of the acoustic wave into the ferromagnetic thin film is thus required. In this work, we therefore propose to study the interaction of *guided* pure shear-horizontal (SH) wave within uniaxial multilayered TbCo<sub>2</sub>/FeCo thin film (in-plane magnetization) deposited on ST-X90°-cut quartz in a delay-line configuration. In our case, the Love wave condition is fulfilled thanks to the chosen ferromagnetic material showing a very high density and softness. Besides enhanced sensitivity, the purpose of this work is to fully understand the SAW coupling occurring in such ferromagnetic thin film, which is rendered easier thanks to the pure shear-horizontal nature of the chosen acoustic wave.

The paper is structured as follows: the magnetoelastic coupling between pure SH wave and a uniaxial nanostructured multilayered magnetostrictive thin film is first described through the equivalent piezomagnetic model in Sec. II. Measurements performed on the fabricated SAW devices are then reported in Sec. III, as well as the comparison with the theoretical data to validate the piezomagnetic model.

## II. THEORETICAL CONSIDERATIONS

### A. SH surface wave in ST-X90°-cut quartz

The ST-cut quartz is a popular piezoelectric material used for decades to design SAW filters, sensors, or temperature-stabilized SAW devices. SAW devices are characterized by three main parameters: phase velocity, electromechanical coupling coefficient ( $K^2$ ), and temperature coefficient of frequency. These parameters usually depend on the substrate orientation and wave-propagation direction, which is here referenced by the angle  $\Psi$ , arbitrarily chosen relatively to the  $x$  axis. A numerical method

that was developed in a previous work [26] to compute the dispersion curves and mode shapes of elastic waves in layered piezoelectric-piezomagnetic composites, is used to obtain the phase velocity and the mode shapes existing in ST-cut quartz [Euler angles ( $0^\circ$ ,  $132.75^\circ$ ,  $\Psi$ )] depending on the propagation direction  $\Psi$ .

The phase velocities of the pure SH mode (magenta) and the Rayleigh wave (blue) are reported in Fig. 1 as a function of the direction of propagation  $\Psi$ .

In order to assess the predominant mode of propagation in such a material depending on the in-plane direction  $\Psi$ , the electromechanical coupling coefficient  $K^2$  is then computed for both modes and is given by

$$K^2 = 2 \frac{v_{CO} - v_{CC}}{v_{CO}}, \quad (1)$$

where  $v_{CO}$  and  $v_{CC}$  are the phase velocities of the open and short circuit boundary condition.  $K^2(\Psi)$  is shown in Fig. 2 for the Rayleigh wave (blue) and the pure SH mode (magenta). The Rayleigh wave is propagating at 3158 m/s for  $\Psi = 0^\circ$  with  $K^2 = 0.14\%$ . For  $\Psi = 90^\circ$ , the solely coupled mode is the pure SH mode (magenta) and shows a phase velocity of 5000 m/s and a  $K^2 = 0.15\%$ . The relative displacement field ( $U_x$ ,  $U_y$ ,  $U_z$ ) of this mode is computed along the propagation direction  $\Psi$  and reported in Fig. 3. It is evident that this mode turns into a pure shear-horizontal mode when  $\Psi = 90^\circ$ , the shear-horizontal component  $U_x$  being the only one to exist. Figure 4 shows that  $U_x$

decreases almost to zero within a depth of  $3\lambda$ . Thus, the SH mode is intrinsically a guided surface acoustic wave, and most of the energy is trapped on the propagation surface with no spurious coupling.

Therefore, the SH mode is only carrying an in-plane unidirectional shear displacement, perpendicular to the direction of propagation. In the following section, the interaction with a magnetostrictive material (multilayered nanostructured TbCo<sub>2</sub>/FeCo) is investigated through the equivalent piezomagnetic model.

## B. Equivalent piezomagnetic model

The equivalent piezomagnetic model was developed previously by the authors to assess magnetoelastic coupling in piezo-electro-magnetic composites (for further details, see Refs. [15,26]). The piezomagnetic equations are obtained by considering a magnetoelastic wave in a ferromagnetic thin film deposited on a piezoelectric substrate or membrane (see Fig. 5), and linearizing the coupled equations for the mechanical and magnetic systems (Newton's equation of motion and Landau-Lifshitz's equation) around a ground-state position of the magnetization (depending on the direction and magnitude of the bias magnetic field).

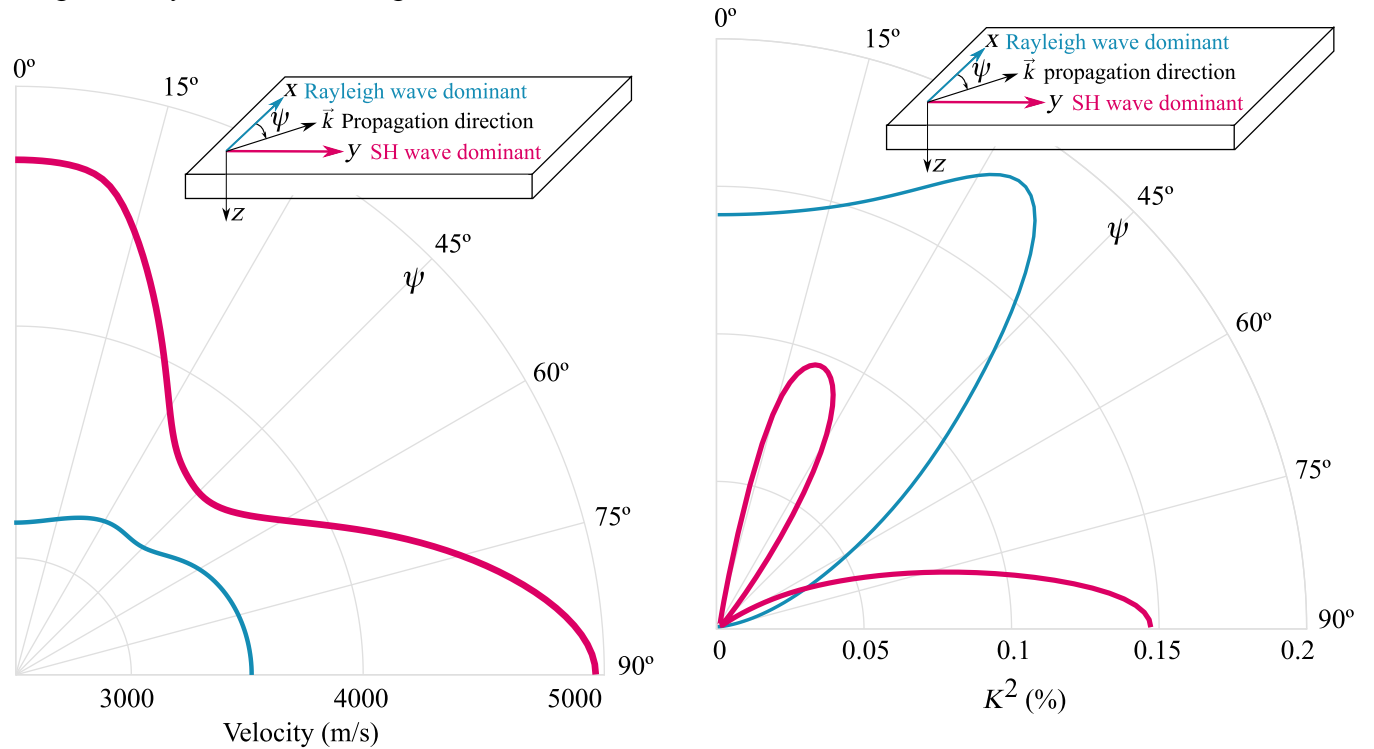


FIG. 1. Phase velocity of the Rayleigh wave (blue) and the pure SH mode (magenta) as a function of the propagation direction  $\Psi$ .

FIG. 2. Electromechanical coupling coefficient  $K^2$  of the Rayleigh wave (blue) and the pure SH mode (magenta) as a function of the propagation direction  $\Psi$ .

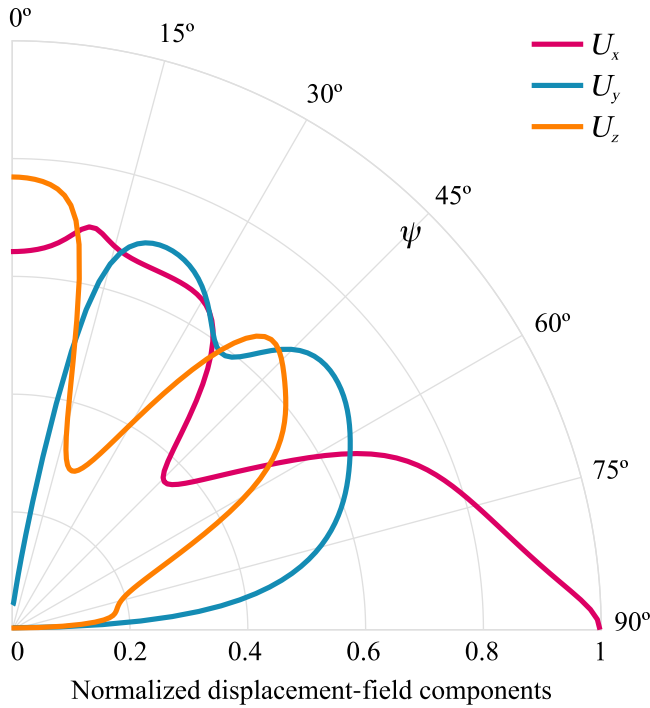


FIG. 3. Displacement field of the SH mode as a function of the propagation direction  $\Psi$ .

In the coordinate system described in Fig. 5 the piezomagnetic equations are given by

$$\rho \frac{\partial^2 u_i}{\partial t^2} = \frac{\partial \sigma_{ij}}{\partial x_j}, \quad (2)$$

$$\frac{\partial b_i}{\partial x_i} = \frac{\partial [\mu_0(h_i + m_i)]}{\partial x_i}, \quad (3)$$

where  $\rho$  is the density of the ferromagnetic thin film,  $u_i$  is the  $i$ th component of the particle displacement,  $x_i$  denotes the Eulerian coordinates (Einstein's summation convention is used,  $i, j, k$ , and  $l = 1, 2, 3$  or equivalently  $x, y, z$ )

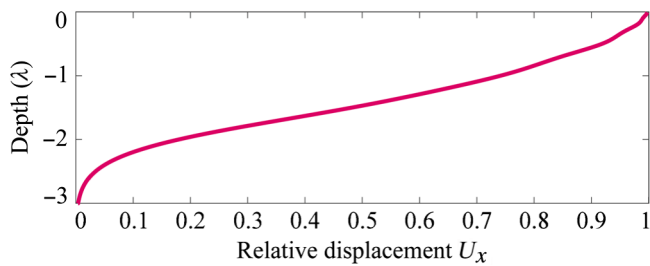


FIG. 4. Relative displacement amplitude  $U_x$  and normalized penetration depth for the SH mode ( $\Psi = 90^\circ$ ).

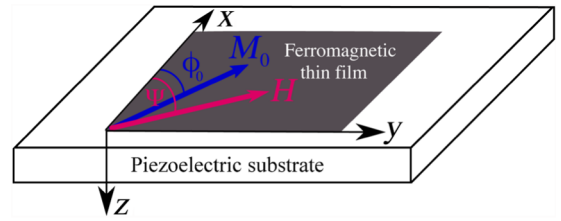


FIG. 5. System coordinates used in the piezomagnetic model.

and

$$\sigma_{ij} = (C_{ijkl} + \Delta C_{ijkl}) \frac{\partial u_k}{\partial x_l} - q_{lij} h_l, \quad (4)$$

$$b_i = q_{ikl} \frac{\partial u_k}{\partial x_l} + \mu_{il} h_l, \quad (5)$$

with  $C_{ijkl}$  the elastic stiffness constants and where the effective magnetic permeability  $\mu_{ij}$  and elastic stiffness constants corrections  $\Delta C_{ijkl}$  are given by

$$\mu_{il} = \mu_0(\delta_{il} + \chi_{il}), \quad (6)$$

$$\Delta C_{ijkl} = b_{ijmn}(M_n^0 q_{mkl} + M_m^0 q_{nkl}), \quad (7)$$

with  $b_{ijkl}$ , the magnetoelastic constants ( $b_{1111} = b^{\nu,2}$  when using Callen's notations [27]). The expressions of the piezomagnetic constants  $q_{ijk}$  and the magnetic susceptibility  $\chi_{il}$  can be found in Ref. [28].

In the following, we consider a uniaxial multilayered  $25 \times [\text{TbCo}_2(3.7 \text{ nm})/\text{FeCo}(4 \text{ nm})]$  nanostructured thin film sputtered under a bias magnetic field ( $C_{11} = 110.9 \text{ GPa}$ ,  $C_{44} = 31.3 \text{ GPa}$ ,  $\rho = 9250 \text{ kg m}^{-3}$ ,  $E = 80 \text{ GPa}$ ,  $b^{\nu,2} = -4.5 \text{ MPa}$ ,  $H_A = 200 \text{ Oe}$ ). The in-plane magnetization is characterized using a vibrating sample magnetometer (VSM), when applying the magnetic field along the  $x$  and  $y$  axis. A clear uniaxial anisotropy is observed as shown on Fig. 6. The  $x$  and  $y$  axis are, respectively, the hard (red) and easy (blue) magnetic axis. The anisotropy field  $H_A$  is estimated to be around 200 Oe. In this study, the bias magnetic field is applied along the hard axis, while the acoustic

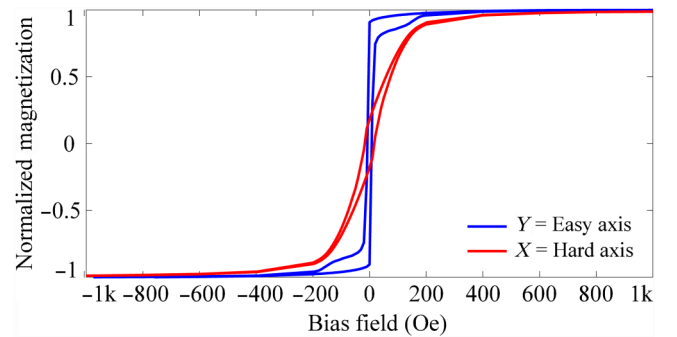


FIG. 6.  $\text{TbCo}_2/\text{FeCo}$  thin-film magnetization characteristics measured along the easy axis (blue) and the hard axis (red).

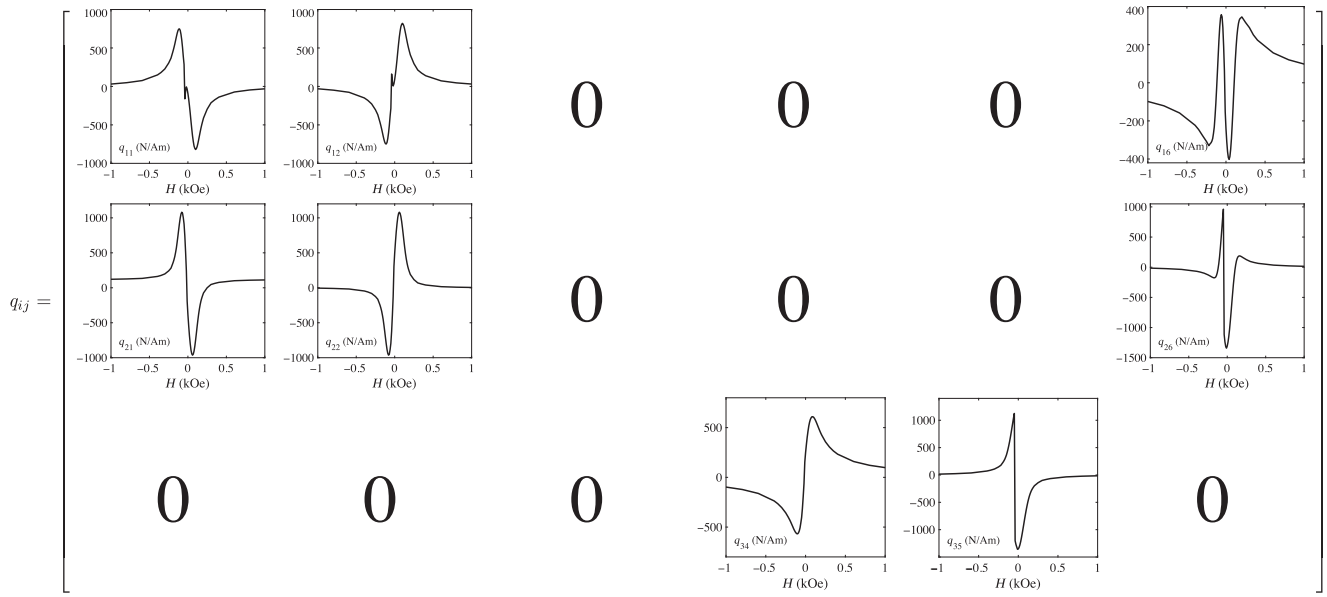


FIG. 7. Magnetic field dependency of the piezomagnetic constant tensor when a bias magnetic field is applied along the hard axis of a multilayered TbCo<sub>2</sub>/FeCo thin film on ST-X90°-cut quartz.

wave propagates along the  $y$  axis. The magnetoelastic coupling induces anisotropy in the magnetostrictive thin film and thus, it cannot be considered as isotropic. The magnetization is supposed to remain always in the plane of the film. For calculations, the magnetic field is applied perpendicular to the easy axis of the magnetostrictive thin film. Its effective elastic constants  $C_{ijkl}$ , piezomagnetic constants  $q_{ijk}$  and relative magnetic permeability constants  $\mu_{ik}$  are computed and reported in Appendix, Figs. 7 and 8, respectively.

The expressions of the elastic stiffness corrections  $\Delta C_{ijkl}$  to  $C_{ijkl}$  due to  $\Delta E$  effect, are given in Table I. In these expressions,  $b^{\nu,2}$  is the magnetoelastic coupling coefficient of the isotropic thin film, and

$$\begin{aligned} U'_{\theta\theta} &= \mu_0 M_s [H_A (1 - \sin^2 \phi_0) + H \cos(\phi_0 - \psi) + H_{ME}], \\ U'_{\phi\phi} &= \mu_0 M_s [H_A (1 - 2 \sin^2 \phi_0) + H \cos(\phi_0 - \psi) + H_{ME}], \end{aligned} \quad (8)$$

where  $H_{ME} = (b^{\nu,2})^2 / (\mu_0 M_s C_{44})$  is the magnetoelastic field,  $\phi_0$  and  $\psi$  the angle with respect to the  $x$  axis with magnetization and magnetic field, respectively. Therefore, the elastic stiffness tensor of the magnetostrictive thin film is modified when biased with a magnetic field and the elastic stiffness constants are modified as follows:

$$\begin{bmatrix} \Delta C_{11} & -\Delta C_{11} & 0 & 0 & 0 & \Delta C_{16} \\ -\Delta C_{11} & \Delta C_{11} & 0 & 0 & 0 & -\Delta C_{16} \\ 0 & 0 & 0 & 0 & 0 & 0 \\ 0 & 0 & 0 & \Delta C_{44} & \Delta C_{45} & 0 \\ 0 & 0 & 0 & \Delta C_{45} & \Delta C_{55} & 0 \\ \Delta C_{16} & -\Delta C_{16} & 0 & 0 & 0 & \Delta C_{66} \end{bmatrix}. \quad (9)$$

The dependency of the overall elastic stiffness constants  $C_{ijkl}$  with respect to the magnetic field is reported in the Appendix.

### C. Analytical resolution for shear-horizontal wave in anisotropic media

In order to enhance the sensitivity of the surface acoustic wave to the magnetostrictive thin-film strain when

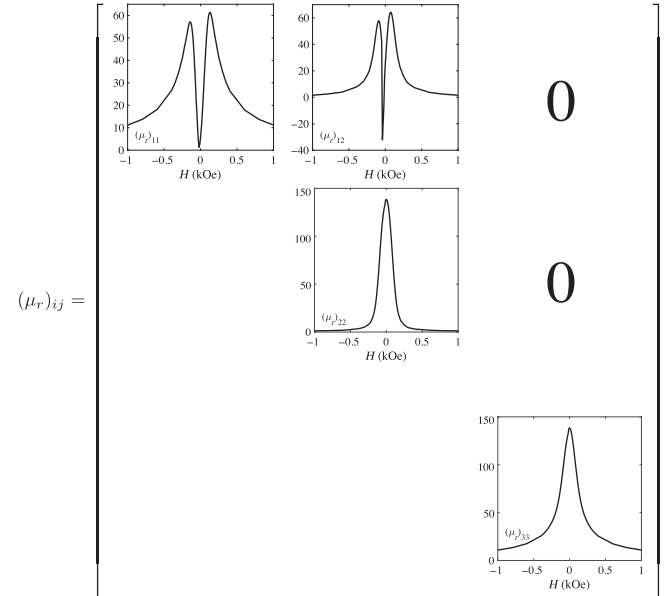


FIG. 8. Magnetic field dependency of the relative magnetic permeability constant tensor when a bias magnetic field is applied along the hard axis of a multilayered TbCo<sub>2</sub>/FeCo thin film on ST-X90°-cut quartz.



TABLE I. Nonzero components of the effective elastic stiffness correction tensor.

$\Delta C_{11} = \frac{-4(b^{\gamma,2})^2 \cos^2 \phi_0 \sin^2 \phi_0}{U'_{\phi\phi}}$	$\Delta C_{16} = \frac{(b^{\gamma,2})^2 \sin(4\phi_0)}{2U'_{\phi\phi}}$
$\Delta C_{44} = \frac{-(b^{\gamma,2})^2 \sin^2 \phi_0}{U'_{\theta\theta}}$	$\Delta C_{45} = \frac{-(b^{\gamma,2})^2 \sin \phi_0 \cos \phi_0}{U'_{\theta\theta}}$
$\Delta C_{55} = \frac{-(b^{\gamma,2})^2 \cos^2 \phi_0}{U'_{\theta\theta}}$	$\Delta C_{66} = \frac{-(b^{\gamma,2})^2 \cos^2(2\phi_0)}{U'_{\phi\phi}}$

biased with a magnetic field, there are essentially three approaches: first, using bulk waves to exploit  $C_{11}$  or  $C_{22}$  variations, through coating of thin piezoelectric plates, or interaction with a Rayleigh wave, mainly sensitive to  $C_{11}$ . Second, manufacturing magnetostrictive thin films with out-of-plane anisotropy to use  $C_{33}$  variations, which is not considered here, since the magnetization remains in plane because of strong demagnetizing effects. Third, using shear surface acoustic waves to take advantage of the  $C_{66}$  dependency with the magnetic field. The latter option is retained, and ST-X90°-cut quartz is chosen for its pure shear-horizontal wave to exploit the induced shear stress and strain of the magnetostrictive thin film.

The velocity dependency with a bias magnetic field of the pure SH mode propagating in this piezo-electromagnetic composite can be easily obtained analytically for anisotropic media considering that both the elastic stiffness matrix of the substrate and ferromagnetic layer are included in the monoclinic system case. The coordinate system and geometry used in this study are depicted in Fig. 9.

For simplicity, the piezoelectricity is neglected. The magnetostrictive layer ( $0 < z < h$ ) is designated as medium (1) with displacement  $u_1^{(1)}(y, z, t)$ , density  $\rho_1$ , and elastic constants  $c_{ij}$  and the half space ( $z \geq h$ ) is designated as medium (2) with displacement  $u_1^{(2)}(y, z, t)$ , density  $\rho_2$ , and elastic constants  $d_{ij}$ . Considering a Love wave ( $u_2 = u_3 = 0$ ) propagating in the positive  $y$  direction with a phase velocity  $c$ , and assuming a  $e^{-j(\omega t - ky)}$  dependence, the displacement field  $u_1$  can be expressed as

$$u_1 = f(z)e^{jk(y-ct)}. \quad (10)$$

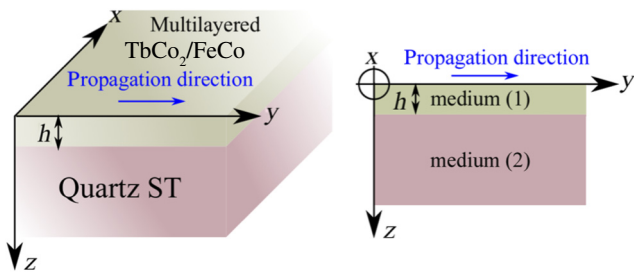


FIG. 9. System coordinates used for the Love-wave device.

Christoffel's tensor-ruling wave propagation in solid media is, therefore, reduced to

$$(\Gamma_{11} - \rho c^2)u_1 = 0, \quad (11)$$

with  $\rho$  the material density,  $c = \omega/k$  the phase velocity, and  $\Gamma_{il} = c_{ijkl}n_j n_k$ ,  $n_m$  being the components of the unit vector in the wave-propagation direction.

The overall equation ruling wave propagation in both materials (condensed notation) is, therefore, given by

$$\rho_{1,2} \frac{\partial^2 u_1}{\partial t^2} = (c, d)_{66} \frac{\partial^2 u_1}{\partial y^2} + 2(c, d)_{56} \frac{\partial^2 u_1}{\partial y \partial z} + (c, d)_{55} \frac{\partial^2 u_1}{\partial z^2}. \quad (12)$$

The general solution of Eq. (12) for the medium (1) is

$$u_1^{(1)} = (A_1 e^{jkb_1 z} + B_1 e^{-jkb_2 z}) e^{jk(y-ct)}, \quad (13)$$

where  $A_1, B_1$  are arbitrary constants and

$$b_1 = (\sqrt{A} - c_{56})/c_{55}, \quad b_2 = (\sqrt{A} + c_{56})/c_{55}, \quad (14)$$

$$A = c_{55}(\rho_1 c^2 - c_{66}) + c_{56}^2.$$

Likewise, given  $\lim_{z \rightarrow \infty} u_1^{(2)} = 0$ , the displacement field  $u_1^{(2)}$  can be expressed as

$$u_1^{(2)} = A_2 e^{jkb_3 z} e^{jk(y-ct)}, \quad (15)$$

with

$$b_3 = \frac{j\sqrt{B} - d_{56}}{d_{55}}, \quad B = d_{55}(d_{56} - \rho_2 c^2) - d_{56}^2, \quad (16)$$

with  $\Im(b_3) > 0$  (i.e.,  $B > 0$ ). The boundary conditions are

$$\tau_{13}^{(1)} = 0 \quad \text{at } z = 0 \text{ (free surface)}, \quad (17)$$

$$u_1^{(1)} = u_1^{(2)} \quad \text{at } z = H \text{ (displacement continuity)}, \quad (18)$$

$$\tau_{13}^{(1)} = \tau_{13}^{(2)} \quad \text{at } z = H \text{ (stress continuity)}. \quad (19)$$

But

$$\tau_{13}^{(1)} = c_{56} \frac{\partial u_1^{(1)}}{\partial y} + c_{55} \frac{\partial u_1^{(1)}}{\partial z}, \quad (20)$$

$$\tau_{13}^{(2)} = d_{56} \frac{\partial u_1^{(2)}}{\partial y} + d_{55} \frac{\partial u_1^{(2)}}{\partial z}. \quad (21)$$

Equations (13)–(19) yield

$$\begin{aligned} A_1 - B_1 &= 0, \\ A_1 e^{jkb_1 h} + B_1 e^{-jkb_2 h} &= A_2 e^{jkb_3 h}, \\ A_1 e^{jkb_1 h} - B_1 e^{-jkb_2 h} &= j \sqrt{\frac{B}{A}} A_2 e^{jkb_3 h}. \end{aligned} \quad (22)$$

Eliminating  $A_1$ ,  $B_1$ , and  $A_2$  in Eq. (22) gives

$$\tan \theta = \sqrt{\frac{B}{A}}, \quad (23)$$

with

$$\theta = \frac{(b_1 + b_2)kh}{2} = \frac{\sqrt{A}}{d_{55}} kh. \quad (24)$$

It can be shown that for Love waves to exist,  $A > 0$ ,  $B > 0$ . Therefore, using Eqs. (14) and (16) the Love-wave dispersion relation may be written as

$$\tan(\gamma \chi_1 kh) = \sqrt{\frac{d_{55} d_{66} \chi_2}{c_{55} c_{66} \chi_1}}, \quad (25)$$

with

$$\gamma^2 = \frac{c_{66}}{c_{55}}, \quad \epsilon_1 = \frac{c_{56}^2}{c_{55} c_{66}}, \quad \epsilon_2 = \frac{d_{56}^2}{d_{55} d_{66}} \quad (26)$$

and the variables  $\chi_1$  and  $\chi_2$  are given by

$$\chi_1 = \sqrt{\frac{c^2}{V_1^2} - 1 + \epsilon_1}, \quad \chi_2 = \sqrt{1 - \epsilon_2 - \frac{c^2}{V_2^2}}, \quad (27)$$

where  $V_1$  and  $V_2$  are the bulk shear velocity in both media and are given by

$$V_1 = \sqrt{\frac{c_{66}}{\rho_1}}, \quad V_2 = \sqrt{\frac{d_{66}}{\rho_2}}. \quad (28)$$

The conditions  $A > 0$  and  $B > 0$  imply

$$\sqrt{1 - \epsilon_1} V_1 < c < \sqrt{1 - \epsilon_2} V_2. \quad (29)$$

In this paper, for the considered magnetostrictive thin film,  $\epsilon_1 = 0$ , since  $c_{56} = 0$ . Moreover, it can be noticed (see Appendix) that it behaves as an elastically isotropic material when saturated with a bias magnetic field, the magnetization being stuck in a well-defined state, the elasticity remains unchanged. In order to take the piezomagnetic effects into account in the analytical Love-wave dispersion

relation, the elastic stiffness constants are rewritten using Eqs. (4) and (5) as

$$C'_{ijkl} = C_{ijkl}^H + \frac{q_{pij} n_p n_q q_{qkl}}{\mu_{mn} n_m n_n}, \quad (30)$$

where  $n_i$  are the components of the wave vector. These enhanced elastic stiffness constants can be used in the Love-wave dispersion relation to obtain the wave velocity dependency with respect to a bias magnetic field. Its evolution is discussed later, along with the characterization of the experimental device in Sec. III C.

### III. EXPERIMENTAL CONSIDERATIONS AND DISCUSSION

#### A. Fabricated SAW delay line

The interaction of the multilayered magnetostrictive thin film with pure shear surface acoustic wave is also investigated experimentally. A SAW delay line is retained as acoustic waveguide. As shown in Figs. 10 and 11 (left), a 300- $\mu\text{m}$ -wide and 200-nm-thick  $(0.016\lambda)25 \times [\text{TbCo}_2(3.7 \text{ nm})/\text{FeCo}(4 \text{ nm})]$  nanostructured uniaxial thin film is deposited by rf sputtering onto a 500- $\mu\text{m}$ -thick ST-cut quartz substrate between two single-electrode aluminum IDTs with a periodicity of 12  $\mu\text{m}$ . The ferromagnetic thin film is deposited under a bias magnetic field to induce the preferred orientation for the magnetization, as seen on Fig. 6. As stated before, the propagation direction of the acoustic wave is along the easy axis (EA) of the ferromagnetic thin film. Transmission electron microscopy on the multilayered nanostructured thin film has been made on a TEM FEI Themis probe corrected, and equipped with a SUPER-X-EDX detector. Imaging is done on STEM mode with the high-angle annular dark-field (HAADF) detector, with which atomic resolution imaging can be achieved (0.07 nm). The resulting picture is reported in Fig. 11 (right), where each  $\text{TbCo}_2/\text{FeCo}$  bilayer can be clearly seen.

#### B. Device characterization and methods

The complex forward transmission  $S_{21}$  of the delay line is measured with a vector network analyzer (Agilent 8753ES) with an input power of  $P = 1 \text{ mW}$ . The acoustic signal resulting from the SAW transmission can be

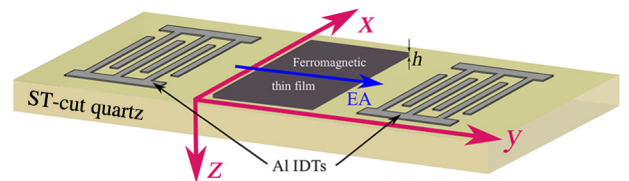


FIG. 10. Three-dimensional (3D) model of the fabricated Love-wave device.

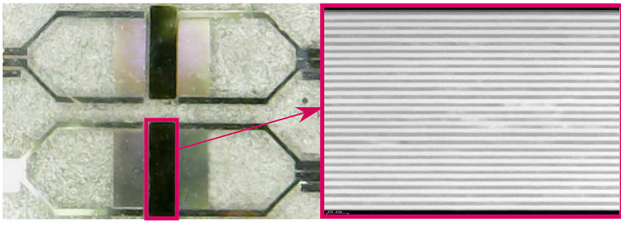


FIG. 11. Photograph of the fabricated SAW delay line: the Al IDTs and the  $\text{TbCo}_2/\text{FeCo}$  multilayered thin film inbetween (left). STEM picture of the multilayered  $\text{TbCo}_2/\text{FeCo}$  nanostructured thin film (overall thickness: 200 nm) deposited on silicon for transmission-electron-microscopy visualization (right).

isolated from spurious signals, including electromagnetic crosstalk and multiple transit signals using Fourier transform and time gating, since the electromagnetic crosstalk is propagating at light speed and the surface acoustic wave is 5 orders of magnitude slower. Therefore, these signals can be separated in time domain. The frequency response of the signal transmitted between the IDTs after thin-film deposition is shown in Fig. 12. The first (SH1) and third harmonic (SH3) of the pure shear-horizontal mode appear clearly on this electrical characteristic at 410 MHz and 1.2 GHz, respectively. In order to characterize the acoustic waveguide when the ferromagnetic thin film is biased with a magnetic field, the magnitude and phase value of the  $S_{21}$  parameter are measured at the frequency showing the lowest insertion loss at zero field.

### C. Study of the SH1 mode at 410 MHz

#### 1. Bias magnetic field applied along the hard axis

In a first set of measurements, the  $S_{21}$  frequency response of the SH1 mode is measured as a function of the bias magnetic field, applied along the hard axis. The normalized phase and amplitude of the insertion loss are depicted in Fig. 13. The amplitude shows a variation of

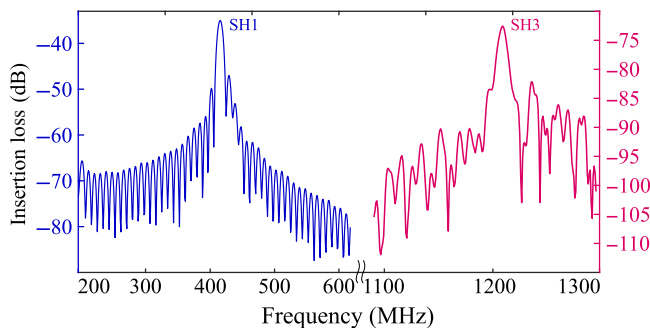


FIG. 12. Frequency response of the realized SAW delay line on  $\text{ST-90}^\circ$  X-cut quartz after deposition of the  $\text{TbCo}_2/\text{FeCo}$  thin film in the frequency range [200–1300] MHz showing the first (SH1) and third harmonics (SH3) of the shear-horizontal mode at zero magnetic field.

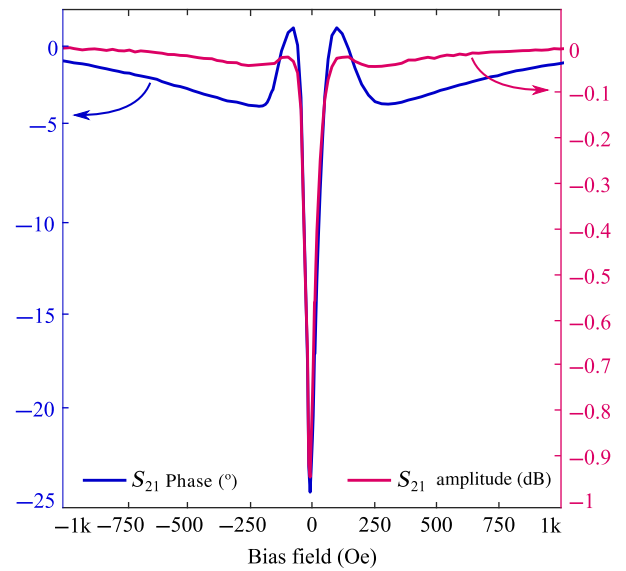


FIG. 13. Complex  $S_{21}$  response (phase in blue, magnitude in magenta) of the SAW delay line operated at 410 MHz as a function of the bias magnetic field applied along the hard axis of the multilayered  $\text{TbCo}_2/\text{FeCo}$  nanostructured thin film.

nearly 1 dB for 100 Oe variation, whereas the phase shift is around  $25^\circ$  for the same magnetic field range. Given the width of the magnetostrictive thin film ( $300 \mu\text{m}$ ), the attenuation reaches 30 dB/cm. The  $S_{21}$  amplitude variation can be explained by the modification of the acoustic impedance  $Z = \rho c$  (with  $\rho$ , the thin-film density and  $c$  the wave-propagation velocity), leading to a variation of the insertion loss with respect to the magnetic field.

The  $S_{21}$  phase shift is converted into a phase velocity shift through the relation

$$\frac{\Delta v}{v} = -\frac{\Delta \Phi}{\Phi}, \quad (31)$$

where  $v$  is the phase velocity and  $\Phi$  is the absolute phase. In Fig. 14, the resulting Love-wave velocity behavior of the SH1 mode (magenta dots) is compared to the Love-wave velocity shift obtained through the dispersion relation (25) by including  $C_{66}$  and  $C_{55}$  magnetic field dependency (blue). One can notice the perfect agreement between the velocity shift obtained with the established Love-wave dispersion relation and the experimental measurements for the SH1 mode. The resulting velocity shift of the Love wave is 0.3% at the fundamental frequency.

A numerical implementation of the equivalent piezomagnetic model is done in COMSOL Multiphysics through the partial differential equation (PDE) module. The 3D unit cell, whose two-dimensional (2D) cut is represented in Fig. 15, is constructed in COMSOL and is composed of a block of ST-cut quartz ( $\lambda$  wide and  $10\lambda$  high) coated with a block of the  $\text{TbCo}_2/\text{FeCo}$  ferromagnetic thin film (200 nm thick). Continuity condition is applied along the  $x$  and



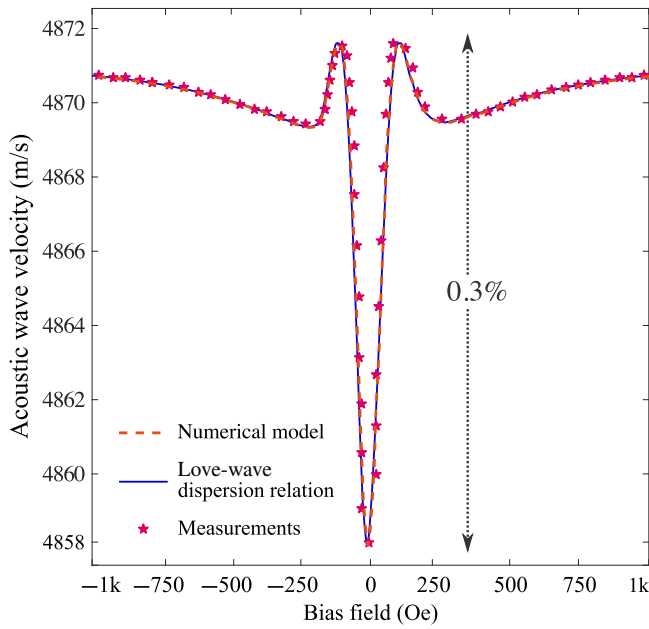


FIG. 14. Comparison between measured  $\text{SH}_1$  phase velocity, phase velocity shift obtained from Love-wave dispersion relation and velocity shift obtained from the FEM model when the multilayered  $\text{TbCo}_2/\text{FeCo}$  thin film is biased along its hard axis at 410 MHz.

$y$  directions and the bottom of the substrate is supposed to be fixed. The behavior of the ferromagnetic thin film with respect to the bias magnetic field is obtained from the equivalent piezomagnetic model described in Sec. II B and implemented as a new material. Therefore, the frequency of the shear eigenmode of the proposed structure is computed as a function of the bias magnetic field. The shear component of the displacement field is depicted in Fig. 15 for the  $\text{SH}_1$  mode. It is clearly shown that the coating with the ferromagnetic thin film (right) enhances the confinement of the acoustic wave in the upper layer compared to the bare ST-cut quartz (left). The penetration depth is reduced by 1:4 at 410 MHz. The induced acoustic wave velocity shift with respect to the bias magnetic field is reported in Fig. 14 and compared to its evolution obtained with the analytical Love-wave dispersion relation (25) and with the experimental measurements. One may notice the good agreement between both methods proving the viability of the FEM tool to deal with the magnetoelastic coupling in more complex structures.

## 2. Influence of the bias magnetic field direction

Magnetic field sensor response to differing bias magnetic field directions relative to the easy axis is investigated. The  $S_{21}$  parameter of the  $\text{SH}_1$  mode is measured for bias magnetic field direction ranging from  $-90^\circ$  to  $90^\circ$  with a step angle of  $10^\circ$  and a magnitude swinging from  $-2000$  to  $2000$  Oe. The phase shift is converted into a

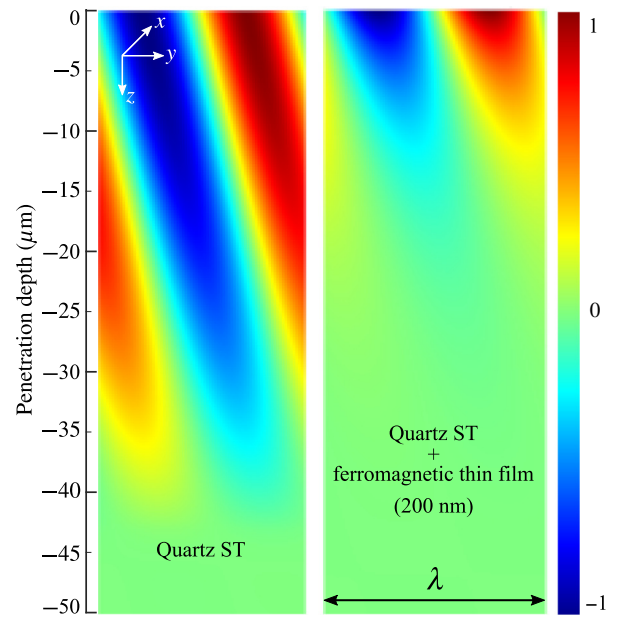


FIG. 15. Normalized shear displacement-field component computed with COMSOL Multiphysics based on the equivalent piezomagnetic model when the ferromagnetic thin film is saturated.

velocity shift with the relation given in Eq. (31) and the result is reported in Fig. 16 for the  $\text{SH}_1$  mode. As highlighted in the inset, as the bias magnetic field orientation gets closer to the hard axis, the velocity variation shows an increasingly recessed “valley-shaped” behavior. This is clearly the signature of the  $\Delta E$  effect [8], the velocity shift owing initial softening of elastic constants and then stiffening as applied field is increased. This valley shape is occurring around the anisotropy field of the multilayered ferromagnetic thin film close to 200 Oe. Indeed, in multilayered  $\text{TbCo}_2/\text{FeCo}$  ferromagnetic thin film exhibiting in-plane uniaxial anisotropy, a high susceptibility to the external driving field can be obtained in the vicinity of a field-induced spin reorientation transition (SRT) [29] when the static external bias magnetic field is applied perpendicular to the easy axis with a magnitude equal to the anisotropy field  $H_A$ . Therefore, for a bias magnetic field close to that value, the elasticity of the magnetostrictive material becomes very soft due to magnetic in-plane rotation, hence the “valley shape.”

## 3. Considerations on Love-wave guiding

Typical Love-wave devices reported in the literature [10,18] usually come with a silicon-dioxide guiding layer deposited on ST-cut quartz to increase the wave confinement thanks to its lower shear velocity (close to 3764 m/s). In that case, the condition (29) for Love wave to exist is fulfilled. In the proposed structure, the multilayered  $\text{TbCo}_2/\text{FeCo}$  thin film acts itself as a very effective guiding layer, its shear velocity being close to 1800 m/s (28),

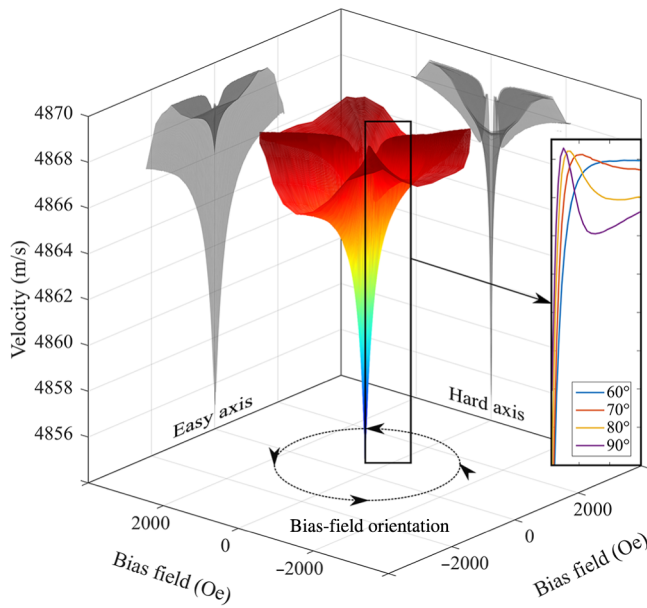


FIG. 16. 3D view of the experimental-phase velocity-shift shape depending on bias magnetic field orientation. The inset shows overlaid cuts of the 3D figure for different orientations of the bias magnetic field. For the measurements carried out along the hard and easy axis, the 3D figure is projected onto a plane (shaded figures) to highlight the velocity-shift sensitivity with respect to the magnetic field.

offering a higher contrast with the substrate shear velocity (close to 5000 m/s), compared to silicon dioxide. A numerical method that was developed in a previous work [26] to compute the dispersion curves and mode shapes of elastic waves in layered piezoelectric-piezomagnetic composites, is used to assess the effect of the ferromagnetic thin-film coating (200 nm) on ST-cut quartz. Fig. 17 reports the shear displacement component of the SH1 and SH3 modes corresponding to differing acoustic wave frequencies. The ferromagnetic layer clearly tends to confine the acoustic wave at the top of the structure. This is even more pronounced as the frequency increases, since the penetration depth is reduced to 1:4 at 410 MHz but 1:8 at 1.2 GHz. In comparison, the same effect is obtained with a 1.8- $\mu\text{m}$ -thick silicon-dioxide coating for the same Love-acoustic-wave velocity. Therefore, the wave energy is mainly confined in the upper layer, improving the surface acoustic wave interaction with the ferromagnetic thin film. Above all, it confirms that the ferromagnetic layer acts as a guiding layer for the acoustic waves.

These preliminary results carried out on the SH1 mode show a very good agreement between the Love-wave dispersion relation, including the equivalent piezomagnetic model and the experimental measurements. As described in Sec. II B, this model considers the magnetoelastic coupling occurring in ferromagnetic thin films and does not take into account any resonant coupling between spin

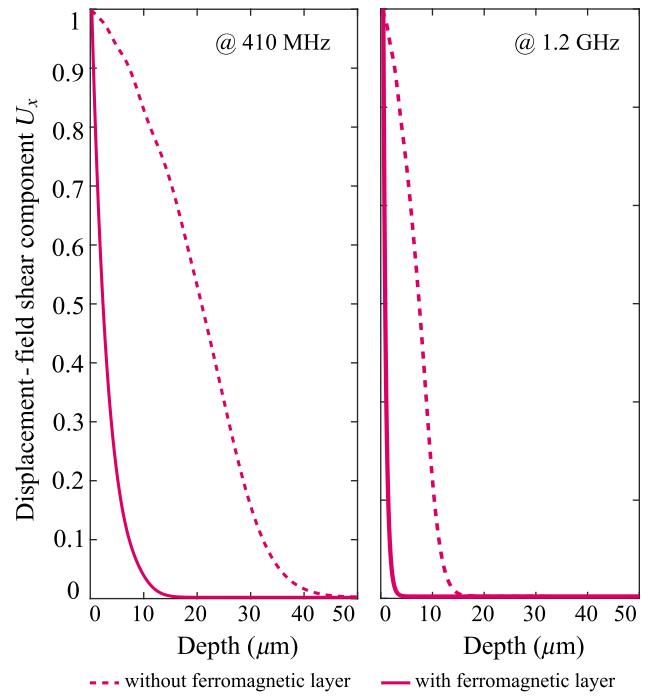


FIG. 17. Comparison of the normalized displacement-field shear component  $U_x$  of the SH mode with or without the ferromagnetic layer coating (TbCo<sub>2</sub>/FeCo) on ST-cut quartz (if present, 200 nm) at two distinct frequencies, 410 MHz (left) and 1.2 GHz (right).

wave and acoustic wave (known as ferromagnetic resonance). The ferromagnetic thin film shows a giant magnetoelastic coupling inducing large wave-propagation velocity shift, but any evidence of the coupling between spin wave and acoustic wave is observed neither for the SH1 nor the SH3 mode. A possible reason may be linked to the hypothetical severe damping occurring in such ferromagnetic thin film, preventing the magnetization precession. Further investigations are required to shed light on the true coupling between dynamic strain and magnetization behavior with respect to the magnetic field. As it stands, a pure magnetoelastic coupling model is perfectly able to explain what is observed experimentally in the proposed Love acoustic waveguide based on a TbCo<sub>2</sub>/FeCo ferromagnetic thin-film guiding layer.

#### D. Study of the SH3 mode at 1.2 GHz

##### 1. Bias magnetic field applied along the hard axis

The frequency response of the acoustic waveguide with respect to the magnetic field is also investigated for the SH3 mode at 1.2 GHz. The normalized phase and amplitude of the insertion loss are depicted in Fig. 18 when the bias magnetic field is applied along the hard axis. The amplitude shows a variation of nearly 15 dB for 100-Oe variation, whereas the phase shift is around 250° (middle) for the same magnetic field range. Given the width of the

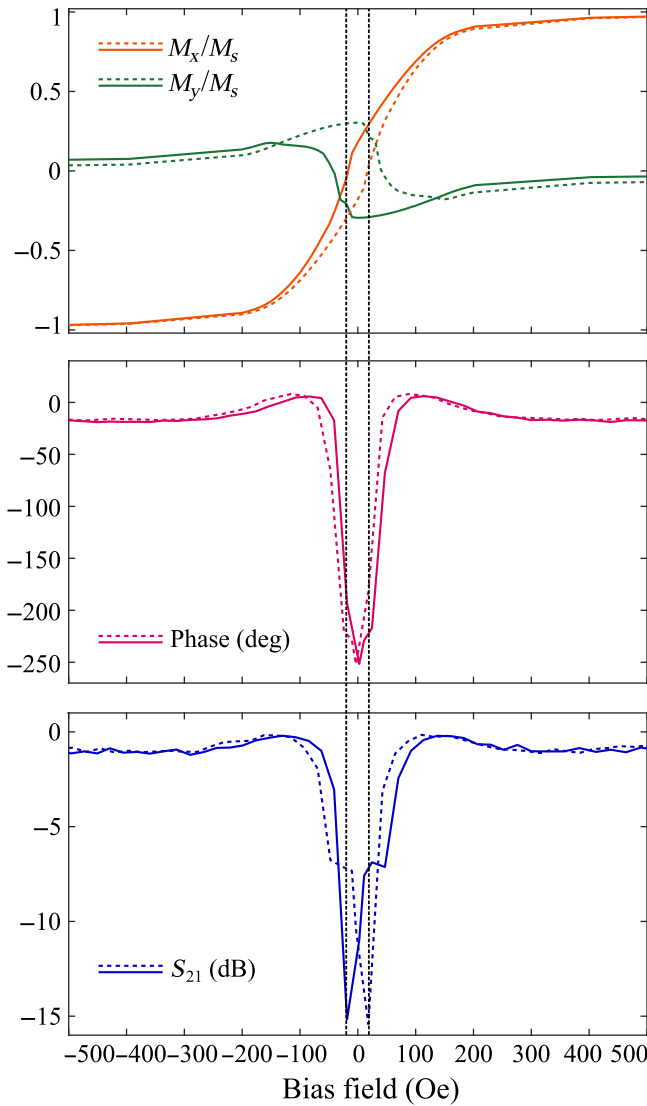


FIG. 18.  $\text{TbCo}_2/\text{FeCo}$  thin-film magnetization characteristics along the hard axis (top). Normalized insertion loss ( $S_{21}$ ) of the SAW delay line at 1.2 GHz [phase (middle) and magnitude (bottom)]. In both figures, the dashed line represents measurements from left to right and solid lines from right to left starting from a saturated state.

magnetostrictive thin film ( $300 \mu\text{m}$ ), the attenuation easily reaches the value of 500 dB/cm (bottom). As a recall, the same measurements performed for the SH1 mode gave only 30 dB/cm of attenuation and  $25^\circ$  of phase shift. The  $S_{21}$  variations with respect to the bias magnetic field are much more pronounced for the SH3 mode, due to a better confinement of the acoustic wave energy in the ferromagnetic thin film (as the frequency increases, the wavelength shortens) and thus, a more effective guiding leads to an increase in sensitivity. One may also notice that the evolution of the  $S_{21}$  parameter with respect to the bias magnetic field is closely related to the magnetization state of the ferromagnetic thin film. Vectorial measurements carried out

on the vibrating sample magnetometer show the full magnetization behavior when biased along the hard axis of the ferromagnetic thin film. As depicted in Fig. 18 (top) where  $M_x$  represents the magnetization along the bias direction (hard axis) and  $M_y$  the simultaneous magnetization along the  $90^\circ$  direction, the magnetization is relaxing towards the easy axis from a saturated state along the hard axis in a “Stoner Wohlfarth” fashion as discussed by Klimov *et al.* [29]. As highlighted in Fig. 18 (black dashed line), the hysteretic nature of the multilayered ferromagnetic thin film is reflected in the  $S_{21}$  amplitude (bottom) and phase (middle). The minima are correlated to the “jump” of the magnetization around zero field, both with increasing or decreasing magnetic field. This “jump” occurring when the magnetization is relaxing from a saturated state along the hard axis corresponds to a brutal reorganization of the magnetization when crossing zero field as discussed by Tiercelin *et al.* [30]. Besides, it can be noticed that the fabricated SAW delay line is behaving like a bipolar magnetic field sensor. Indeed, the  $S_{21}$  magnitude shows a crossing with opposite slope around zero field. Therefore, the SAW device is able to sense the direction of small magnetic field without any polarization.

## 2. Acoustic mode conversion and limitations of the analytical Love-wave dispersion relation

The Love-wave velocity shift obtained experimentally or the SH3 mode is reported in Fig. 19 (magenta stars). The maximum velocity shift reaches 2.5%, which corresponds, as the film thickness is only 0.8% of the acoustic wavelength, to a variation of the elastic properties of the ferromagnetic thin film close to 100%. One may further note that the “valley shape” around the anisotropy field ( $H_A = 200 \text{ Oe}$ ) is less recessed compared to the SH1 mode. The comparison between the experimental measurements and the velocity shift obtained with the Love-wave dispersion relation reported in Fig. 19 (blue curve) shows that the analytical dispersion relation is not as accurate as it is for the SH1 mode to depict the evolution of the velocity with respect to the magnetic field close to the anisotropy field  $H_A$  (200 Oe).

Precisely, the analytical Love-wave dispersion relation (25) is obtained assuming that pure shear-horizontal wave is propagating in the ferromagnetic thin film. This assumption is true in ST-cut quartz (intrinsic to the material), but not completely when coated with the anisotropic ferromagnetic material. Indeed, as depicted in Fig. 20, the normalized displacement-field components of the studied acoustic wave depend on the magnetic state of the ferromagnetic thin film and the frequency of operation. More precisely, it is shown that the ferromagnetic layer behaves as an isotropic layer when saturated and thus, the acoustic wave is pure shear (left). When the ferromagnetic thin film is not biased (zero field), its anisotropy gives birth to

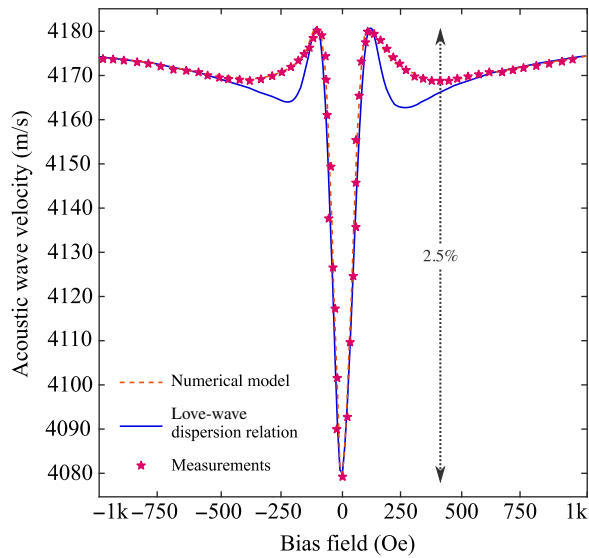


FIG. 19. Comparison between measured SH3 phase velocity, velocity shift obtained from Love-wave dispersion relation, and velocity shift obtained from the numerical model when the multilayered TbCo<sub>2</sub>/FeCo thin film is biased along its hard axis at 1.2 GHz.

a three-component displacement field leading to a breaking of the acoustic wave polarization. As the frequency increases (middle and right), the two additional components become non-negligible and show more pronounced effect on the acoustic wave response with respect to the bias magnetic field. Precisely, for the SH3 mode, the contribution of the second component  $U_y$  plays a role in the magnetoelastic coupling through the  $C_{12}$  elastic stiffness constant, showing opposite behavior compared to  $C_{66}$  with respect to the magnetic field around the anisotropy field (200 Oe) as reported in the Appendix. It may explain that the “valley shape” is less recessed at 1.2 GHz, the  $C_{12}$  contribution compensating the effect of the  $C_{66}$ . The anisotropic nature of the ferromagnetic thin film depending on the bias magnetic field, the acoustic wave polarization is linked to the bias magnetic field and therefore can lead to an acoustic mode conversion depending on the ferromagnetic thin-film thickness and the acoustic wave frequency.

Therefore, the complete displacement-field vector must be taken into consideration in order to depict the real behavior of the Love acoustic wave with respect to the magnetic field. For that purpose, the implemented numerical model in COMSOL Multiphysics can be used to compute the acoustic wave velocity shift as a function of the bias magnetic field. The results obtained with the numerical model are reported in Fig. 19, showing a good agreement with the experimental data. One might further note that the velocity is lower as the frequency increases, proving that the acoustic wave is even more guided in the upper ferromagnetic layer, the velocity getting closer to the bulk

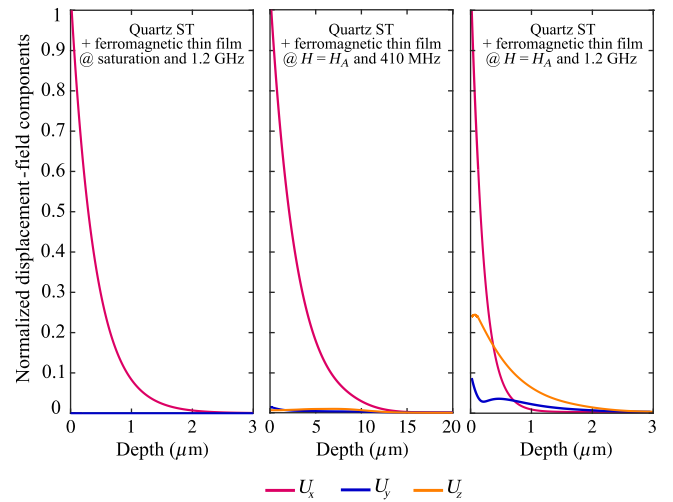


FIG. 20. Comparison of the normalized displacement-field components of the SH mode for [ST-cut quartz + TbCo<sub>2</sub>/FeCo multilayer (200 nm)] at two distinct bias magnetic field, saturation field (left) and anisotropy field at 410 MHz (middle) and 1.2 GHz (right).

shear velocity of the ferromagnetic thin film. Therefore, a frequency increase by a factor of 3 leads to an increase of the sensitivity by a factor of roughly 10. This behavior is explained by the dispersive nature of the Love wave as the frequency increases. In order to assess the potential of the presented Love acoustic waveguide in terms of velocity shift with respect to the bias magnetic field (and thus, the sensitivity), the analytical dispersion relation is used. Using Eq. (25), the maximum Love-wave velocity shift with respect to the magnetic field is computed as a function of the ratio between the ferromagnetic film thickness  $h$  and the acoustic wavelength  $\lambda$ . The maximum Love-wave

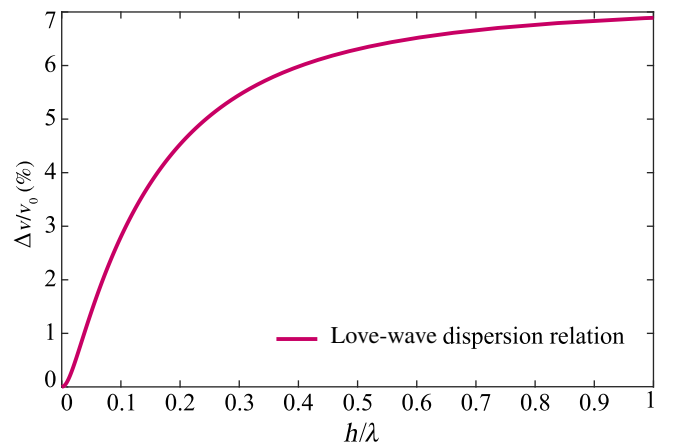


FIG. 21. Love-wave velocity shift with respect to the magnetic field as a function of the ratio between the ferromagnetic film thickness and the acoustic wavelength.

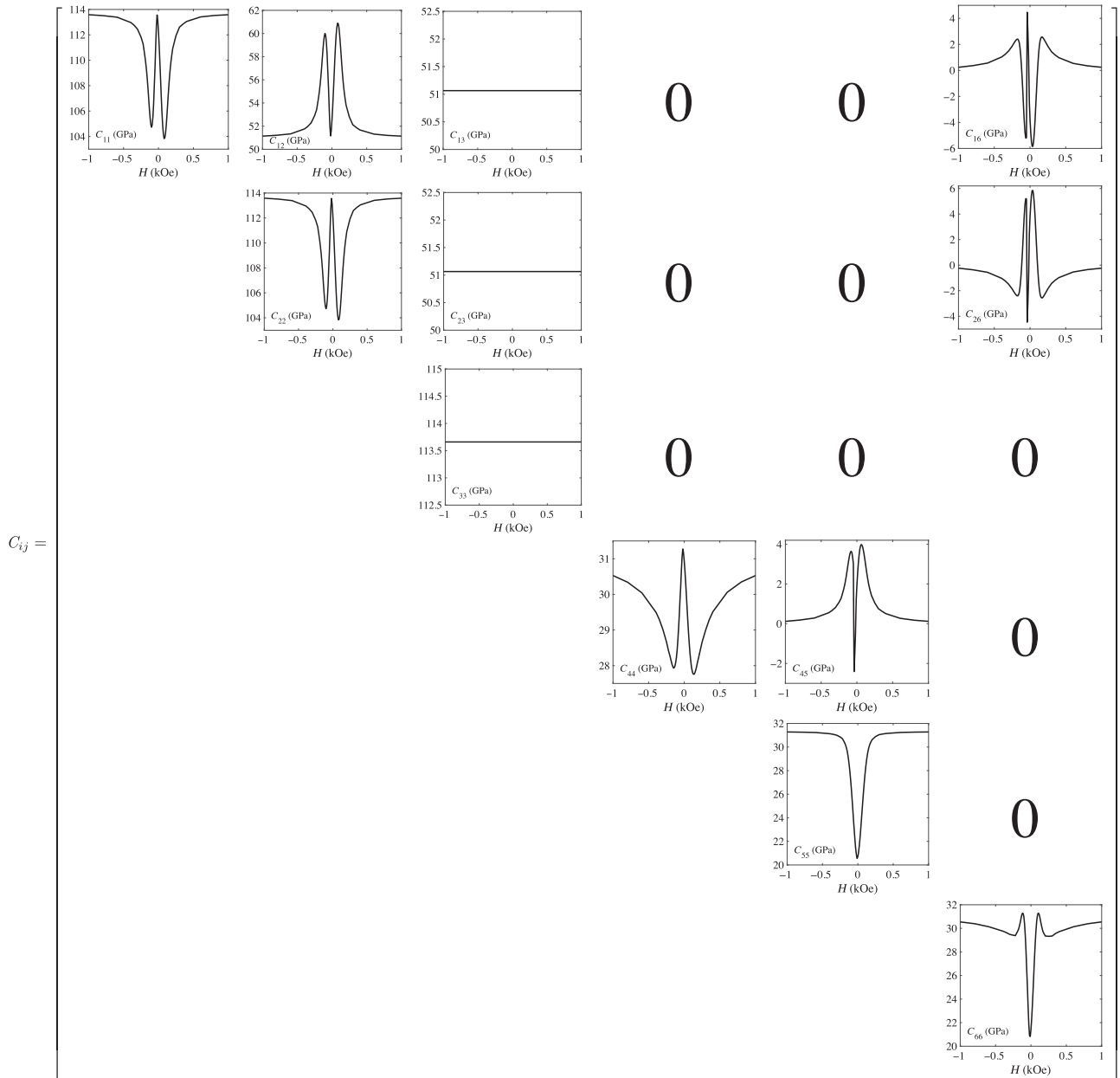


FIG. 22. Magnetic field dependency of the elastic stiffness constant tensor when a bias magnetic field is applied along the hard axis of a multilayered  $\text{TbCo}_2/\text{FeCo}$  thin-film ST-X90°-cut quartz.

velocity shift is assessed using the relation (32):

$$\frac{\Delta v}{v_0} = \frac{v_{\max} - v_{\min}}{v_{\max}}. \quad (32)$$

The resulting sensitivity is depicted in Fig. 21. The maximum relative Love-wave velocity shift is close to 7% for a ratio  $h/\lambda$  close to 1. The fabricated Love-wave device reported in Sec. III, shows only a ratio  $h/\lambda$  close to 0.016, leaving room for improvement to design a highly sensitive magnetic field sensor. The analytical approach has the advantage of providing a complete understanding of the

physical coupling, but the need of the global numerical model is required to take into account the true nature of the wave polarization as the frequency increases due to the anisotropic nature of the ferromagnetic thin film. The validity of the proposed equivalent piezomagnetic model proves to be satisfying even when working with complex wave polarization.

#### IV. CONCLUSION

We present here a thorough investigation, both theoretical and experimental, of giant magnetoelastic coupling in Love acoustic waveguides. The existence of



guided acoustic waves in a TbCo<sub>2</sub>/FeCo ferromagnetic thin film on ST-X90°-cut quartz is demonstrated. The use of guided acoustic waves shows an exalted sensitivity by 1 order of magnitude compared to evanescent waves in conventional piezoelectric substrates. At a fundamental level, the proposed single-mode structure allows a complete understanding of the magnetoelastic coupling in such ferromagnetic materials and the development of an equivalent piezomagnetic model based on pure magnetoelastic coupling is used to assess the induced velocity shift due to  $\Delta E/G$  effect. Measurements performed on a SAW delay line coated with a uniaxial multilayered TbCo<sub>2</sub>/FeCo nanostructured thin film are compared with very good agreement to the predictions of the model for the SH1 and SH3 modes. A maximum velocity shift of 2.5% is reached for the SH3 mode. The attenuation induced by the ferromagnetic thin film in this configuration easily reached 500 dB/cm. The reported theoretical model and experimental results are of tremendous interest for the development of advanced devices for magnetic field sensing applications as well as investigating magnon-phonon interaction at a fundamental level. Finally, resonant coupling between magnon-phonon is not observed in our structure but may further improve the sensitivity.

### ACKNOWLEDGMENTS

The authors thank the support of the Agence Nationale de la Recherche through Grant No. 2010 BLAN 923 0, RENATECH NETWORK and Centrale Lille through PhD fellowship.

### APPENDIX

The evolution of the elastic stiffness constants  $C_{ijkl}$  of the ferromagnetic thin film with respect to the magnetic field is numerically computed using Eq. (7) and Table I and is reported in Fig. 22. The magnetization state of the ferromagnetic thin film is taken into account through experimental measurements and implemented in the model. The reported results are obtained for a bias magnetic field applied along the hard axis of the ferromagnetic thin film.

---

[1] J. Zhai, S. Dong, Z. Xing, J. Li, and D. Viehland, Geomagnetic sensor based on giant magnetoelectric effect, *Appl. Phys. Lett.* **91**, 1 (2007).  
 [2] J. Ou-Yang, X. Liu, H. Zhou, Z. Zou, Y. Yan, J. Li, Z. Yue, B. Zhu, S. Chen, and X. Yang, Magnetoelectric laminate composites: An overview of methods for improving the DC and low-frequency response, *J. Appl. Phys. D* **51**, 324005 (2019).  
 [3] T. Nan, Y. Hui, M. Rinaldi, and N. X. Sun, Self-biased 215 MHz magnetoelectric NEMS resonator for ultra-sensitive DC magnetic field detection, *Sci. Rep.* **3**, 1 (2013).

[4] Y. Hui, T. Nan, N. X. Sun, and M. Rinaldi, High resolution magnetometer based on a high frequency magnetoelectric MEMS-CMOS oscillator, *J. Microelectromech. Syst.* **24**, 134 (2015).  
 [5] A. Piorra, R. Jahns, I. Teliban, J. L. Gugat, M. Gerken, R. Knöchel, and E. Quandt, Magnetoelectric thin film composites with interdigital electrodes, *Appl. Phys. Lett.* **103**, 032902 (2013).  
 [6] Z. Sárközi, K. Mackay, and J. C. Peuzin, Elastic properties of magnetostrictive thin films using bending and torsion resonances of a bimorph, *J. Appl. Phys.* **88**, 5827 (2000).  
 [7] A. Ludwig and E. Quandt, Optimization of the  $\Delta E$  effect in thin films and multilayers by magnetic field annealing, *IEEE Trans. Magn.* **38**, 2829 (2002).  
 [8] W. P. Robbins and A. Hietala, A simple phenomenological model of tunable SAW devices using magnetostrictive thin films, *IEEE Trans. Ultrason. Ferroelectr. Freq. Control* **35**, 718 (1988).  
 [9] W. Wang, Y. Jia, X. Xue, Y. Liang, and Z. Du, Grating-patterned FeCo coated surface acoustic wave device for sensing magnetic field, *AIP Adv.* **8**, 015134 (2018).  
 [10] A. Kittmann, P. Durdaut, S. Zabel, J. Reermann, J. Schmalz, B. Spetzler, D. Meyners, N. X. Sun, J. Mccord, M. Gerken, G. Schmidt, M. Höft, R. Knöchel, F. Faupel, and E. Quandt, Wide band low noise love wave magnetic field sensor system, *Sci. Rep.* **8**, 278 (2018).  
 [11] W. Y. Li, P. Dhagat, and A. Jander, Surface acoustic wave magnetic sensor Using galfenol thin film, *IEEE Trans. Magn.* **48**, 4100 (2012).  
 [12] D. W. Forester, C. Vittoria, D. C. Webb, and K. L. Davis, Variable delay lines using magnetostrictive metallic-glass film overlays, *J. Appl. Phys.* **49**, 1794 (1978).  
 [13] D. C. Webb, K. L. Davis, N. C. Koon, and A. K. Ganguly, Magnetoelastic surface wave propagation in a low-anisotropy rare-earth-iron compound at 80 MHz, *Appl. Phys. Lett.* **31**, 245 (1977).  
 [14] M. Elhosni, O. Elmazria, S. Petit-watelot, L. Bouvot, M. Hehn, A. Talbi, N. Tiercelin, V. Preobrazhensky, P. Pernod, and O. Boumatar, in *IEEE International Ultrasonics Symposium (IUS)* (2014), p. 874.  
 [15] H. Zhou, A. Talbi, N. Tiercelin, and O. Bou Matar, Multilayer magnetostrictive structure based surface acoustic wave devices, *Appl. Phys. Lett.* **104**, 114101 (2014).  
 [16] V. Polewczyk, K. Dumesnil, D. Lacour, M. Moutaouekkil, H. Mjahed, N. Tiercelin, S. Petit Watelot, H. Mishra, Y. Dusch, S. Hage-Ali, O. Elmazria, F. Montaigne, A. Talbi, O. Bou Matar, and M. Hehn, Unipolar and Bipolar High-Magnetic-Field Sensors Based on Surface Acoustic Wave Resonators, *Phys. Rev. Appl.* **8**, 024001 (2017).  
 [17] P. Smole, W. Ruile, C. Korden, A. Ludwig, E. Quandt, S. Krassnitzer, and P. Pongratz, in *Proceedings of the 2003 IEEE International Frequency Control Symposium and PDA Exhibition Jointly with the 17th European Frequency and Time Forum*, (2004), p. 903.  
 [18] X. Liu, J. Ou-Yang, B. Tong, S. Chen, Y. Zhang, B. Zhu, and X. Yang, Influence of the delta-E effect on a surface acoustic wave resonator, *Appl. Phys. Lett.* **114**, 062903 (2019).  
 [19] M. Kadota and S. Ito, Sensitivity of surface acoustic wave magnetic sensors composed of various Ni electrode structures, *Jpn. J. Appl. Phys.* **51**, 3 (2012).

- [20] M. Elhosni, S. Petit-Watelot, M. Hehn, S. Hage-Ali, K. A. Aissa, D. Lacour, A. Talbi, and O. Elmazria, Experimental study of multilayer piezo-magnetic SAW delay line for magnetic sensor, *Procedia Eng.* **120**, 870 (2015).
- [21] L. Dreher, M. Weiler, M. Pernpeintner, H. Huebl, R. Gross, M. S. Brandt, and S. T. B. Goennenwein, Surface acoustic wave driven ferromagnetic resonance in nickel thin films: Theory and experiment, *Phys. Rev. B* **86**, 134415 (2012).
- [22] D. Labanowski, A. Jung, and S. Salahuddin, Effect of magnetoelastic film thickness on power absorption in acoustically driven ferromagnetic resonance, *Appl. Phys. Lett.* **111**, 102904 (2017).
- [23] J. Duquesne, P. Rovillain, C. Hepburn, M. Eddrief, P. Atkinson, R. Ranchal, M. Marangolo, J. Duquesne, P. Rovillain, C. Hepburn, M. Eddrief, and P. Atkinson, Sub-GHz Resonant Magnetoelastic Coupling in Epitaxial Fe Thin Films, hal-02022637 (2019).
- [24] L. Thevenard, C. Gourdon, J. Y. Prieur, H. J. von Bardeleben, S. Vincent, L. Becerra, L. Largeau, and J.-Y. Duquesne, Surface-acoustic-wave-driven ferromagnetic resonance in (Ga, Mn)(As, P) epilayers, *Phys. Rev. B.* **90**, 094401 (2014).
- [25] M. Weiler, L. Dreher, C. Heeg, H. Huebl, R. Gross, M. S. Brandt, and S. T. B. Goennenwein, Elastically Driven Ferromagnetic Resonance in Nickel Thin Films, *Phys. Rev. Lett.* **106**, 117601 (2011).
- [26] O. Bou Matar, N. Gasmi, H. Zhou, M. Goueygou, and A. Talbi, Legendre and Laguerre polynomial approach for modeling of wave propagation in layered magneto-electro-elastic media, *J. Acoust. Soc. Am.* **133**, 1415 (2012).
- [27] E. R. Callen and H. B. Callen, Static magnetoelastic coupling in cubic crystals, *Phys. Rev.* **129**, 578 (1963).
- [28] O. Bou Matar, J. F. Robillard, J. O. Vasseur, A.-C. Hladky-Hennion, P. A. Deymier, P. Pernod, and V. Preobrazhensky, Band gap tunability of magneto-elastic phononic crystal, *J. Appl. Phys.* **111**, 54901 (2012).
- [29] A. Klimov, N. Tiercelin, V. Preobrazhensky, and P. Pernod, Inhomogeneous spin reorientation transition (SRT) in giant magnetostrictive TbCo<sub>2</sub>/FeCo multilayers, *IEEE Trans. Magn.* **42**, 3090 (2006).
- [30] N. Tiercelin, J. B. Youssef, V. Preobrazhensky, P. Pernod, and H. L. Gall, Giant magnetostrictive superlattices: From spin reorientation transition to MEMS. Static and dynamical properties, *J. Magn. Magn. Mater.* **249**, 519 (2002).